Math. Model. Nat. Phenom. **12** (2017) 208–225
https://doi.org/10.1051/mmnp/2017065

Mathematical Modelling of Natural Phenomena
www.mmnp-journal.org

PATCHY, NOT PATCHY, OR HOW MUCH PATCHY? CLASSIFICATION OF SPATIAL PATTERNS APPEARING IN A MODEL OF BIOLOGICAL INVASION

N. Petrovskaya[1], S. Petrovskii[2] and W. Zhang[1]

Abstract. Good understanding of spatiotemporal patterns of species spread during biological invasion is needed for efficient monitoring and control of harmful alien pests. Various growth-dispersal-type models of population dynamics predict that invasive species spread can follow two qualitatively different scenarios such as the propagation of a continuous population front and the "no-front" patchy invasion. Distinguishing between these two patterns of spread is important, in particular because the patchy invasion poses a much greater challenge for monitoring and control. However, a mathematical theory of the patchy invasion is missing and it remains unclear what are the restrictions on parameter values and how much different this dynamical regime is from the continuous front propagation. In this paper, we address these issues in terms of a biologically meaningful mathematical model consisting of two coupled integral-difference equations. We show that the relevant domain of the parameter space has a complex intermittent structure. We also suggest a criterion that can be used to distinguish between the patchy invasion and the continuous front propagation: the patchy-invasion spatial pattern is shown to be much more sensitive to the cutoff at low densities.

Mathematics Subject Classification. 92D40, 35B36, 35Q92, 37N25.

Received June 28, 2017. Accepted October 28, 2017.

1. Introduction

For a species in natural environment, the spatial distribution of its population density is rarely homogeneous. The population spatial distribution often forms a complicated "patchy" multiscale pattern where areas with high population density alternates with areas where the population density is low or the species is absent at all. This phenomenon, often referred to as patchiness [15], is known to have a variety of implications for the population dynamics as well as the population management, monitoring and control [16, 28, 34]. A number of theories have been suggested to explain the patchiness [29]. Some of them link it to exogenous factors such as heterogeneity of the environment [3, 7] while others relate it to endogenous biological interactions [8, 10, 23, 38, 41]; in a general and/or more realistic case, both endogenous and exogenous factors are likely to contribute [12, 35, 39]. The appreciation of ecological patchiness is, however, relative rather than absolute and conclusions are often made based on a rule of thumb. Mathematical approaches allowing for classification of the patterns (*e.g.* to answer the questions whether a given pattern is actually patchy, not patchy or "how much patchy") are largely

Keywords and phrases: patchy invasion, patchy spread, pattern formation, predator-prey system.

[1] School of Mathematics, University of Birmingham, Birmingham, UK. n.b.petrovskaya@bham.ac.uk
[2] Department of Mathematics, University of Leicester, Leicester, UK.

Article published by EDP Sciences

absent, although attempts to address this issue using statistical measures were made in the contexts of plankton dynamics [5] and landscape ecology [47].

Mechanisms resulting in the patchy dynamics, as well as the implications of the spatial patterning, can be context-specific. In this paper, we focus on the pattern formation induced by biological invasion [10, 18, 41, 42]. Mathematically, the specifics of population dynamics during invasion is due to the choice of the initial conditions belonging to a certain class (*e.g.* described by a function with a finite support). Our special attention is on the "patchy invasion" [31, 32] which can be generically described as the spread of the alien population from the place of its introduction without formation of a continuous population front. Propagation of a population front was a paradigm of biological invasion for several decades [6, 13, 44]. In the realistic 2D case, such a front forms a continuous boundary separating the invaded and non-invaded areas [2]. More recently, however, there have been a growing understanding that the invading species can proliferate into space by creating isolated patches or colonies but without forming any continuous population front [31, 43]. Patchy invasion, as this invasion scenario was eventually named, is a phenomenon of considerable theoretical and practical importance; it has been observed in several field studies [4, 19, 20, 22] and in a variety of different[1] mathematical models [17, 25, 43] including PDEs [9, 26] and, recently, integral-difference equations [37]. Despite the intense study of patchy invasion in recent years, its full understanding and a consistent mathematical theory are still missing and there are many open questions. Patchy invasion is known to occur inside a particular parameter domain (where the corresponding non-spatial population invariably goes to extinction [23, 32]) but little is known about the fine structure of the parameter domain [9, 30]. Identification of relevant parameters is, however, very important for the purposes of monitoring and control. In this paper, our first goal is to make an insight into this issue using a biologically meaningful system of integral-difference equations [14, 37].

Our second goal is to quantify the patchiness itself. One general problem in comparing predictions of a mathematical-ecological model to empirical data is that they often operate with variables of different origin. Mathematical models are routinely formulated in terms of the population density. Meanwhile, a direct estimation of the population density in field studies is rarely possible. For instance, monitoring of insects is usually done with traps; however, trap counts interpretation is challenging and can be ambiguous. The same trap count can arise in a high density population of slowly moving insects and in a low density population of fast moving insects [33, 34], *cf.* the so called "activity-density paradigm" [45]. Also, trap's efficiency is limited: in case of a low population density, *i.e.* below a certain detection threshold, after the time of its exposition the trap is likely remain empty even if the monitored population is actually present. For this and other reasons, the data of empirical studies are usually available as presence/absence maps rather than maps of the population density. In mathematical terms, it means implementation of a certain threshold or cutoff: whenever the population density is lower than a given value, it is regarded as zero. Immediate questions arising here are (a) how this cutoff may change the properties of the pattern (*e.g.* turning a simply-connected domain to a multi-connected one) and (b) what are the values of the cutoff when such a change happens and how these values may depend on the population dynamics parameters. In this paper, we endeavor to provide an insight into the above issues.

The paper is organized as follows. In the next section, we formulate the mathematical model and briefly outline the numerical method to solve it. In Section 3, we introduce a classification of spatial patterns and reveal the corresponding structure of the parameter space by performing extensive numerical simulations. In Section 4, we consider the sensitivity of the patterns to the cutoff. Section 5 provides a discussion and concluding remarks.

2. Model and method

Consider a system of two species N and P that are engaged into an agonistic interaction such as prey-predator or host-parasitoid. Let species N be the prey (host) and P be its predator (parasitoid). We consider the case where the life cycle of both species exhibits two distinctly different stages (as often happens with plants and

[1] We mention here that the relevance of some of the models may be limited to a particular spatial scale, *e.g.* the stochastic spread [17] is more relevant on the small spatial scale of individuals and individual movement whilst the coupled map lattices [25] are more relevant to the large regional/landscape scale.

insects). The first one is the demographic stage which can include growth of juveniles, their maturation, mating and reproduction. We assume that the timing of this stage is the same for both species and that during this stage the species interact (*i.e.* as prey and predator or host and parasitoid). The second stage is dispersal[2] and we assume that the species disperse independently of each other.

The above biological settings are best taken into account by a time-discrete framework [14]. The species are described by their population densities that evolve from generation t to generation $t+1$. Let $N_t(\mathbf{r})$ and $P_t(\mathbf{r})$ be densities of the prey and the predator in generation t over continuous 2D space, $\mathbf{r} = (x, y)$. For convenience of interpretation only (but see [21]), we assume that the species first go through the demographic stage and then disperse. The prey-predator dynamics during the demographic stage is generically described by the following equations:

$$\widetilde{N}_t(\mathbf{r}) = f(N_t(\mathbf{r}), P_t(\mathbf{r})), \quad \widetilde{P}_t(\mathbf{r}) = g(N_t(\mathbf{r}), P_t(\mathbf{r})), \tag{2.1}$$

where N_t and P_t are the species spatial distributions emerging after the dispersal stage in the previous generation.

Since most of the results of this study will be obtained in numerical simulations, we have to choose a specific parametrization for the demographic functions f and g. Following [36, 37] we choose them as follows:

$$f(N_t, P_t) = \frac{A(N_t)^2}{1 + B^2(N_t)^2} \cdot \exp(-\kappa P_t), \tag{2.2}$$

$$g(N_t, P_t) = \delta N_t P_t \ , \tag{2.3}$$

where $A > 0$ is the prey intrinsic growth rate, $(1/B) > 0$ is the prey density for which its per capita growth rate reaches its maximum, $\kappa > 0$ is the predator efficiency and $\delta > 0$ quantifies the predator growth rate. The non-convex shape of the dependence of f on N means that the prey growth is affected by a strong Allee effect. For a detailed discussion of the rationale behind the expressions (2.2)–(2.3) see [36].

It is convenient to introduce dimensionless densities N' and P' as

$$N'_t = \delta/\kappa N_t \quad \text{and} \quad P'_t = \kappa P_t. \tag{2.4}$$

The dimensionless functions f and g are then

$$f(N_t, P_t) = \frac{a(N_t)^2}{1 + b(N_t)^2} \cdot \exp(-P_t), \tag{2.5}$$

$$g(N_t, P_t) = N_t P_t \ , \tag{2.6}$$

where the primes are omitted for the sake of simplicity. The demographic parameters $a = A\kappa/\delta$ and $b = (B\kappa/\delta)^2$ in (2.5)–(2.6) determine steady states of (2.1), *i.e.* the extinction state $s_1 = (0, 0)$, two prey-only states $s_2 = (N_1^*, 0)$ and $s_3 = (N_2^*, 0)$, and the coexistence state $s_4 = (N^*, P^*)$, where

$$N_1^* = \frac{a - \sqrt{a^2 - 4b}}{2b} \ , \quad N_2^* = \frac{a + \sqrt{a^2 - 4b}}{2b} \ , \tag{2.7}$$

$$(N^*, P^*) = \left(1, \ln\left[\frac{a}{b+1}\right]\right). \tag{2.8}$$

[2]The part of the life cycle where the dispersal takes place depends on the species traits. For instance, many insect species disperse as adults; on the contrary, the plant species usually disperse as offsprings (*i.e.* seeds).

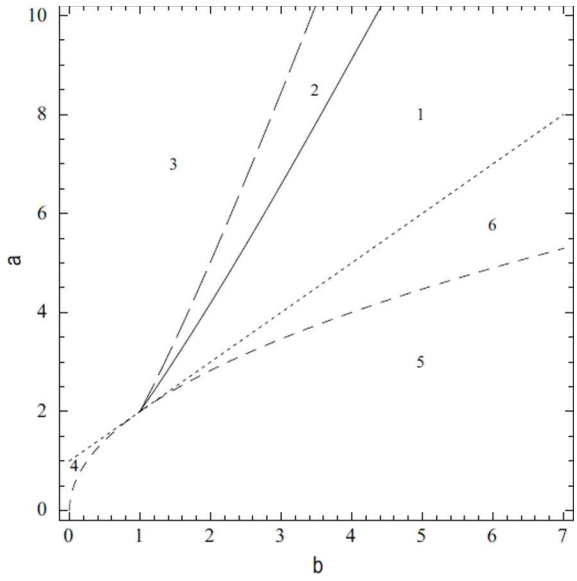

FIGURE 1. The structure of the parameter plane for system (2.5)–(2.6); see details in the text.

While the extinction state s_1 always exists, the boundary states s_2 and s_3 are only feasible for $a > 2\sqrt{b}$. Similarly, the coexistence state s_4 is only feasible for $b+1 < a$. The linear stability analysis reveals that s_1 is always stable, s_2 is always unstable, and s_3 is stable for

$$2 < a < b + 1, \tag{2.9}$$

so that condition $b > 1$ is required for stability [36]. The coexistence equilibrium s_4 is stable for

$$a \;<\; a_{cr} \;=\; (b+1)\exp\left(\frac{b-1}{b+1}\right). \tag{2.10}$$

The structure of the parameter plane (b, a) is shown in Figure 1. The coexistence state s_4 is feasible and stable for parameters from Domain 1. The solid curve in Figure 1 corresponds to $a = a_{cr}$ in equation (2.10) where the coexistence state (N^*, P^*) loses its stability through the Hopf bifurcation; on the line $a = a_{cr}(b)$ the determinant of the Jacobian matrix at the coexistence equilibrium is equal to one [1]. Inside Domain 2 the local dynamics is oscillatory according to the (multipoint) limit cycle. When crossing the long-dashed curve (obtained numerically), the limit cycle disappears so that in Domain 3 the only attractor is the extinction state. The straight dotted line corresponds to $a = b+1$ in equation (2.9); therefore, for Domains 4, 5 and 6 the coexistence state is not feasible. In particular, in Domain 5, the only steady state is $(0, 0)$. The short-dashed curve corresponds to $a = 2\sqrt{b}$ in equation (2.7) and in Domains 4 and 6 the two "prey only" states exist. The prey only equilibrium $(N_1^*, 0)$ is never stable, while $(N_2^*, 0)$ is stable for parameter values inside Domain 6. We therefore observe that in Domains 1 and 6 the system exhibits bistability.

After the demographic stage of the given generation is complete, the species enter the dispersal stage which, when finished, produces the species spatial distribution in the next generation:

$$N_{t+1}(\mathbf{r}) = \int_\Omega \widetilde{N}_t(\mathbf{r}')\; k_N(\mathbf{r}, \mathbf{r}')\mathrm{d}\mathbf{r}', \quad P_{t+1}(\mathbf{r}) = \int_\Omega \widetilde{P}_t(\mathbf{r}')\; k_P(\mathbf{r}, \mathbf{r}')\mathrm{d}\mathbf{r}', \tag{2.11}$$

where Ω is a dispersal domain whose definition is discussed later. The dispersal kernel k_i, $i = N, P$ in equation (2.11) is the probability density function of the event that an individual moves from position $\mathbf{r}'$ to position $\mathbf{r}$ after dispersal. In this paper, we consider the Gaussian dispersal kernel given by

$$k_i(\mathbf{r}, \mathbf{r}') \equiv k_i(|\mathbf{r} - \mathbf{r}'|) = \frac{1}{2\pi\alpha_i^2} \exp(-\frac{|\mathbf{r} - \mathbf{r}'|^2}{2\alpha_i^2}), \quad i = N, P, \tag{2.12}$$

where the standard deviation α_i is the parameter quantifying the spatial scale of the dispersal.

Having substituted (2.1) into (2.11), we exclude the variables $\widetilde{N}_t$ and $\widetilde{P}_t$ and obtain the following system of integro-difference equations:

$$N_{t+1}(\mathbf{r}) = \int_\Omega k_N\left(|\mathbf{r} - \mathbf{r}'|\right) f\left(N_t\left(\mathbf{r}'\right), P_t\left(\mathbf{r}'\right)\right) \mathrm{d}\mathbf{r}', \tag{2.13}$$

$$P_{t+1}(\mathbf{r}) = \int_\Omega k_P\left(|\mathbf{r} - \mathbf{r}'|\right) g\left(N_t\left(\mathbf{r}'\right), P_t\left(\mathbf{r}'\right)\right) \mathrm{d}\mathbf{r}'. \tag{2.14}$$

System (2.13)–(2.14) is a generic model of the two-stage time-discrete spatiotemporal population dynamics. In the below, it is used with the dispersal kernels defined as (2.12) and the demographic functions given by (2.5)–(2.6).

Equations (2.13)–(2.14) are considered in the infinite domain $\Omega = \{(x, y) : -\infty < x < \infty,\ -\infty < y < \infty\}$ to produce the solution for prey density $N_{t+1}(\mathbf{r})$ and predator density $P_{t+1}(\mathbf{r})$ subject to some initial conditions. In our work we consider the two following types of the initial conditions.

– symmetrical initial conditions. The prey population is distributed in some sub-domain centered around the origin and the predator is present in a smaller region also centered around the origin:

$$N_0(x, y) = N_2^* \ \text{ for } \ -1 \le x \le 1 \ \text{ and } \ -1 \le y \le 1, \quad \text{and } \ N_0(x, y) = 0 \ \text{ otherwise}, \tag{2.15}$$

$$P_0(x, y) = P^* \ \text{ for } \ -0.1 \le x \le 0.1 \ \text{ and } \ -1 \le y \le 1, \quad \text{and } \ P_0(x, y) = 0 \ \text{ otherwise}, \tag{2.16}$$

where N_2^* is the prey equilibrium density in the absence of the predator and P^* is the predator equilibrium density in the predator-prey system; see equations (2.7)–(2.8).

The initial conditions (2.15)–(2.16) are obviously invariant with regards to the reflection $x \to -x$ and $y \to -y$, and hence the mathematical problem as a whole, *i.e.* equations (2.13)–(2.14) with (2.15)–(2.16), attains this reflectional symmetry as well. The emerging distributions of prey and predator are hence expected to be symmetrical, too. While this special case can be conveniently exploited for validation of the model, it is not entirely realistic. Correspondingly, in order to make the simulation results more general, along with (2.15)–(2.16) we consider the initial population distribution without any apparent symmetry;

– asymmetrical initial conditions. The prey population is distributed in the same sub-domain as above, but the predator population is now initially distributed in an acentric region:

$$N_0(x, y) = N_2^* \ \text{ for } \ -1 \le x \le 1 \ \text{ and } \ -1 \le y \le 1, \quad \text{and } \ N_0(x, y) = 0 \ \text{ otherwise}, \tag{2.17}$$

$$P_0(x, y) = P^* \ \text{ for } \ -1 \le x \le 0.2 \ \text{ and } \ -0.9 \le y \le 0.4, \quad \text{and } \ P_0(x, y) = 0 \ \text{ otherwise}. \tag{2.18}$$

Having chosen the initial conditions, the solution to equations (2.13)–(2.14) cannot be obtained in closed form and we seek an accurate numerical approximation to the analytical solution instead. The original infinite domain is replaced with a finite domain $\Omega = \{(x, y) : -L \leq x \leq L,\ -L \leq y \leq L\}$ where a numerical solution is considered. It is required that linear size L of domain Ω is large enough for accurate approximation of the solution in the finite domain. For a sufficiently large L, the numerical solution should not be sensitive to the conditions at the external boundary of domain Ω, should any boundary condition be required [37]. If L is chosen to be insufficiently large then "boundary forcing" may occur and the population dynamics inside the domain may be affected by the boundary conditions. We mention here that, unlike partial differential equations, the integral-difference equations (2.13)–(2.14) do not necessarily require any boundary condition to ensure that the problem is well-defined. For a detailed discussion of this issue see [37] where also recommendations have been given on the choice of L required to keep the approximation error within desired accuracy. For the rest of this paper we assume that L is large enough to provide a correct numerical solution, *i.e.* the inherent dynamics of the system is not affected by the boundary conditions.

Once the original infinite domain has been replaced with a finite domain, we employ the Fast Fourier Transform (FFT) method for numerical solution of equations (2.13)–(2.14) along with the initial conditions (2.15)–(2.16) or (2.17)–(2.18). In our computation we choose the linear size of domain Ω as $L = 20$. In order to apply the FFT, the continuous space was first discretized by introducing a numerical mesh. It was then checked in numerical simulations that the mesh steps are chosen sufficiently small in order to exclude any significant numerical artifacts. The parameters of the dispersal kernels are chosen as $\alpha_N = 0.1$ and $\alpha_P = 0.125$ and the other parameters are varied according to the purpose of our study. Further details of the FFT implementation for the system (2.13)–(2.14) (including the accuracy of the method) can be found in our previous work [37].

3. Results I: Pattern formation

The main goal of our study is to investigate how the scenario of species spread during biological invasion – in particular, the spatial pattern of the density distribution emerging as a result of the spread – depends on the demographic parameters a and b in equations (2.5)–(2.6). In doing this, we focus on the spatial distributions of prey $N(x, y)$; yet our conclusions readily apply to the spatial distribution of predator $P(x, y)$ because it exhibits similar properties.

3.1. Spatial patterns and their classification

In a prey-predator system where the prey is affected by the strong Allee effect, there are two baseline options for the evolution of the compact initial conditions, *i.e.* the populations either go extinct or they proliferate into space. This dichotomy is well studied in terms of reaction-diffusion models (*cf.* Chap. 12 in [23]) but other growth-dispersal models exhibit qualitatively similar behavior; *e.g.* see [25, 37], also [18]. Since the extinction of prey is a somewhat trivial result, and indeed our goal here is to understand the properties of the patterns generated by the species spread, the parameters α_N and α_P, and the initial conditions (2.15)–(2.16) and (2.17)–(2.18) are chosen in such a way so that to exclude this option.

In case the initial abundance of prey is large enough to ensure its survival, usually it starts spreading into space (sometimes after a certain time lag that can be caused by a purely dynamical mechanisms, *e.g.* see Sect. 3.5 in [18]). How this spread actually takes place (with or without pattern formation, with or without continuous population front, etc.) is known to a large extent depend on the properties of the non-spatial system (*e.g.* whether the positive steady state is stable or unstable) and hence depends on the demographic parameters a and b. We mention here that, to the best of our knowledge, a dynamical switching between the patterns has never been observed; whatever the spatial pattern emerging in the course of spread is, it will remain qualitatively the same at any time (excluding only very early stage when the shape of the initial distribution can have an effect). For this reason and for the sake of brevity, every scenario of species spread discussed below is represented by a single snapshot.

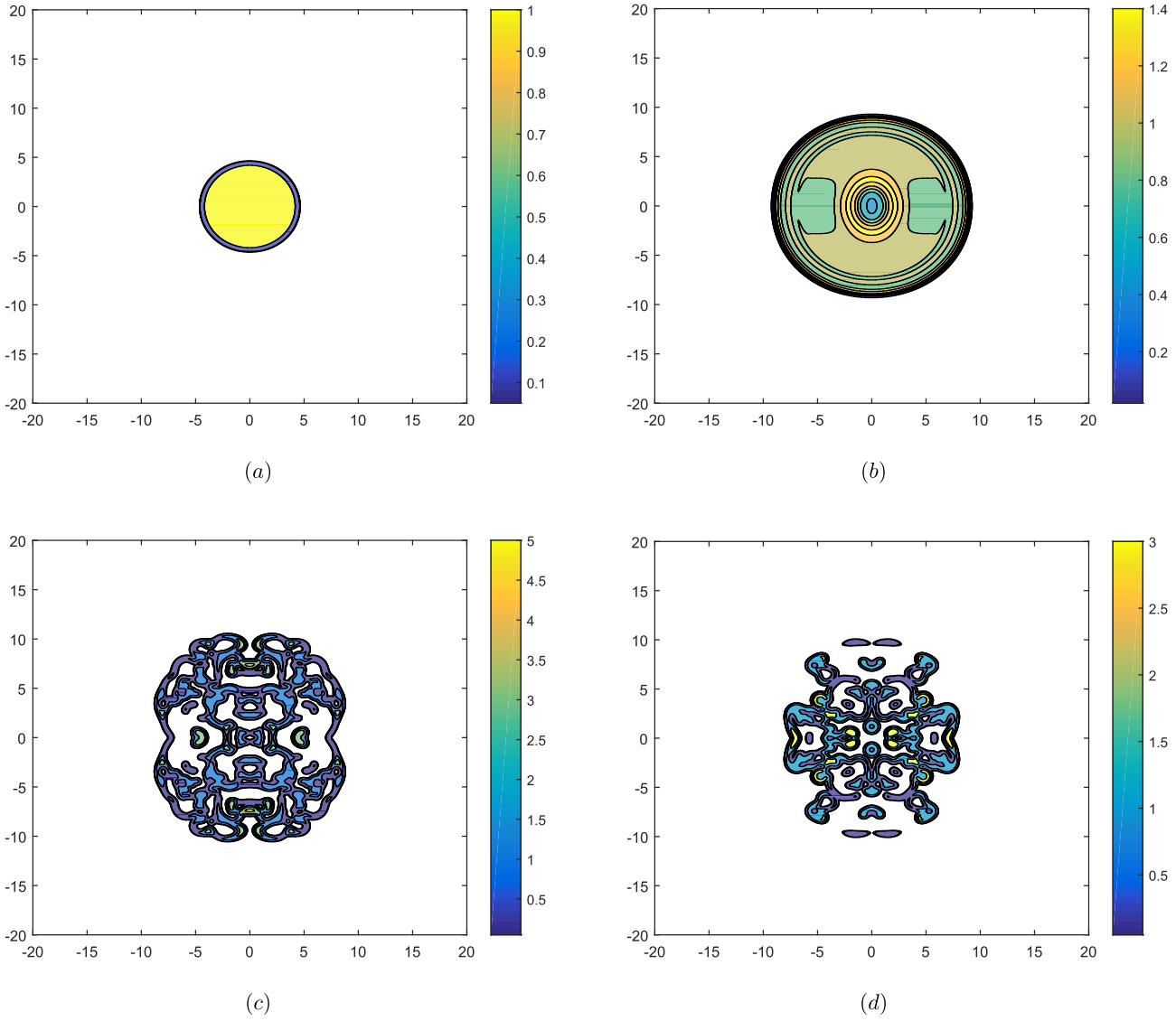

FIGURE 2. Snapshots of the spatial density distribution at time $t = 200$ (obtained for initial conditions (2.15)–(2.16) and different values of parameters a and b) representing different invasion scenarios. White color corresponds to the zero population density. (a) Convex continuous front with a uniform distribution in the wake obtained for parameters taken from Domain 1 (see Fig. 1) as $a = 4.0$ and $b = 2.8$; (b) convex continuous front with pattern formation in the wake obtained for parameters taken from Domain 2 as $a = 4.0$ and $b = 1.8$; (c) concave continuous front obtained for parameters taken from Domain 3 as $a = 4.0$ and $b = 0.716$; (d) patchy spread (without any continuous front) obtained for parameters $a = 4.0$ and $b = 0.714$ (also from Domain 3).

Consider the parametric plane shown in Figure 1. For any parameters from Domain 1, the temporal dynamics is stable meaning that in the large-time limit the solution of the non-spatial counterpart of (2.13)–(2.14) converges to the stable positive equilibrium (N^*, P^*). As a result, the population density remains constant behind the propagation front. An example of a spatial density distribution where parameters a and b are taken in Domain 1 is shown in Figure 2a where symmetric initial conditions (2.15)–(2.16) have been used. In the figure,

the prey spatial density $N(x, y)$ is shown at time $t = 200$ for parameters $a = 4.0$ and $b = 2.8$. We will label this spatial pattern as a "convex continuous front".

For any parameters from Domain 2, the temporal dynamics is oscillatory. An example of a spatial density distribution where parameters $a = 4.0$ and $b = 1.8$ are taken in Domain 2 is shown in Figure 2b. Again, we use the symmetric initial conditions and the prey density is shown at time $t = 200$. It can be seen from the figure that the density $N(x, y)$ exhibits strong spatial oscillations behind the front. (This phenomenon is well known in relevant reaction-diffusion models, *e.g.* see [23, 40].) In the context of this study, however, we consider the density pattern shown in Figure 2b to be the same type as the one shown in Figure 2a because from a "topological" viewpoint it also exhibits a convex continuous front.

The population dynamics becomes different and more sophisticated when parameters a and b are taken from Domain 3. The only attractor is then the extinction state. It means that in the corresponding non-spatial system the species goes extinct. In the spatially explicit system (2.13)–(2.14), the species can survive and even eventually spread over space. However, the pattern of spread depends on the sub-domain of Domain 3 where the parameters are taken from. When parameters are close to the right-hand side boundary of Domain 3 (a long-dashed curve in Fig. 1) we still have a convex continuous front (not shown here for the sake of brevity) topologically similar to that observed for parameters from Domain 2. This pattern of spread changes when the parameters move away from the domain boundary (*e.g.* by decreasing b). Successful invasion *via* the propagation of the convex population front eventually changes to extinction. This transition occurs not abruptly but through a few topological changes, *cf.* Figures 2c and 2d. The first of them is a shape that we label as a concave continuous front. The example of such a spatial pattern is shown in Figure 2c where time is $t = 200$ and parameters are $a = 4.0$ and $b = 0.716$ in Domain 3. Unlike a standard convex topology of continuous fronts in Figures 2a and 2b, for a straight line connecting any two points in the region behind the front, the whole of the line does not necessarily belong entirely to that region. It is important to note, however, that we still deal with a continuous front because a domain of the non-zero population density has a closed boundary.

Let us further decrease the value of b to obtain a spatial pattern shown in Figure 2d for $a = 4.0$, $b = 0.714$ and $t = 200$. This spatial pattern is very different from the density distributions discussed above as it presents a collection of separate patches of the non-zero density. The population density is high inside the patches and is very close to zero between the patches. Apparently, there is no continuous boundary separating the areas with zero and non-zero density and the population spreads over the space as an agglomeration of several different patches. Propagation of such spatial distributions over the physical domain with time was called "patchy invasion" in [25, 26, 31, 32] (as the prey was considered as an invasive species in the original work [31]). Correspondingly, we label this spatial structure as "patchy density distribution". We want to emphasize that the patchy distribution shown in Figure 2d is not at all unique as a similar patchy spread (*i.e.* not preceded by the propagation of a continuous population front) can be observed for other parameter values taken in Domain 3 of the (b, a) parametric plane.

In conclusion to this section, we have checked whether the patchy pattern arising as a result of the population spread (*e.g.* see the middle of the domain in Figs. 2c and 2d) is a self-sustained dynamics or just a slow, long transient extinction. Recall that for those parameter values the extinction is the only issue in the corresponding non-spatial system. Since an analytical theory of the patchy dynamics is not available, we checked its persistence in long term computer simulations. We observed that the patchy dynamics persists at least until $t = 2000$ (a longer simulation is not practically possible as it requires huge computer time). Taken together with similar results available for the patchy dynamics in reaction-diffusion systems (where the persistence was demonstrated up to $t = 10^5$), it indicates that the patchy spatiotemporal pattern is a sustainable dynamics of the system (2.13)–(2.14).

3.2. Structure of the parametric plane

In the previous section, we have identified three topologically different patterns of the population spread during biological invasion, *cf.* Figures 2b–2d, arising as solutions of system (2.13)–(2.14) with compact initial conditions given by (2.15)–(2.16). Interestingly, all three different patterns can be observed for parameters taken

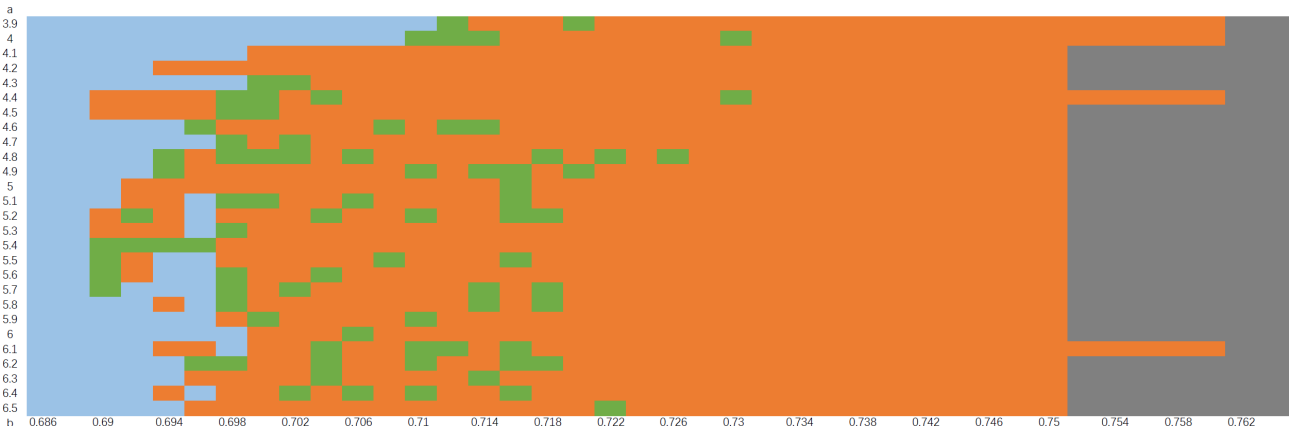

FIGURE 3. The fine structure of Domain 3. Parameter resulting in different spatial patterns are color-coded as follows: blue for the extinction, orange for a concave continuous front, grey for a convex continuous front, green for the patchy invasion (no continuous front).

from the same domain of the parameter plane, *i.e.* Domain 3. (Note that parameter Domains 1 and 2 define the pattern of spread in a unique way.) Obviously, it means that, in the case that the positive steady state (N^*, P^*) is unstable, the properties of the spatial system cannot be predicted based on the properties of its non-spatial reduction. The question therefore arises as to what is the "fine structure" of Domain 3, *e.g.* how often each pattern of spread appears when we vary parameters a and b in Domain 3. We are especially interested in parameter values that result in a patchy spread. Indeed, any information about conditions required for formation of patchy spatial patterns is of particular value as their ecological monitoring and control can be very different from the monitoring protocol for continuous front population density distributions.

In order to make an insight into the fine structure of Domain 3, we perform intense numerical simulations. Both parameters a and b are varied inside Domain 3 with a small increment. In order to make the simulation results obtained for different parameter values consistent and comparable, for any pair (b, a) we pick up the solution obtained at the particular time $t = 200$; having analyzed the numerical solutions at different times and different parameters, this time was deemed to be sufficient for the dynamical regime to establish. For all values of a and b used in the simulations, the spatial pattern obtained at $t = 200$ is then labeled according to the classification suggested in the previous section. We mention it here that, having chosen the specific moment $t = 200$ to reveal the solution properties and performing the simulations in the spatial domain of a fixed size $L = 20$, for technical reasons we have to limit our study to a certain parameter range. In particular, as the rate of spread depends on a and b, values $a > 6.5$ are not feasible as, for those values, by $t = 200$ the solution has already approached the boundary of the spatial domain and it is not possible to robustly identify the pattern.

The results of our simulations performed for $b \in [0.686, 0.766]$ and $a \in [3.9, 6.5]$ are summarized in Figure 3 where a color-coding is used to represent different patterns of spread. Blue-colored regions show the parameter range for which the populations go to extinction. Green-colored regions present the parameter range where the patchy spread is observed. Orange-colored regions show the parameter range for which a concave continuous front has been formed. Finally, grey-colored regions show the parameter range where the population spread takes place *via* the propagation of a convex continuous front. For parameter values outside this range, we observe extinction for any value of b when $a < 3.9$.

The results of Figure 3 demonstrate that, in a certain sub-domain of Domain 3, the evolution of initial conditions (2.15)–(2.16) results in a wealth of invasion patterns; the population spread can occur either by the propagation of a continuous population front, convex or concave, or by the dynamics of separate population patches. When changing parameters (*e.g.* to increase b), the "standard" propagation pattern of convex continuous front first turns into a concave front before completely breaking down into agglomeration of separate

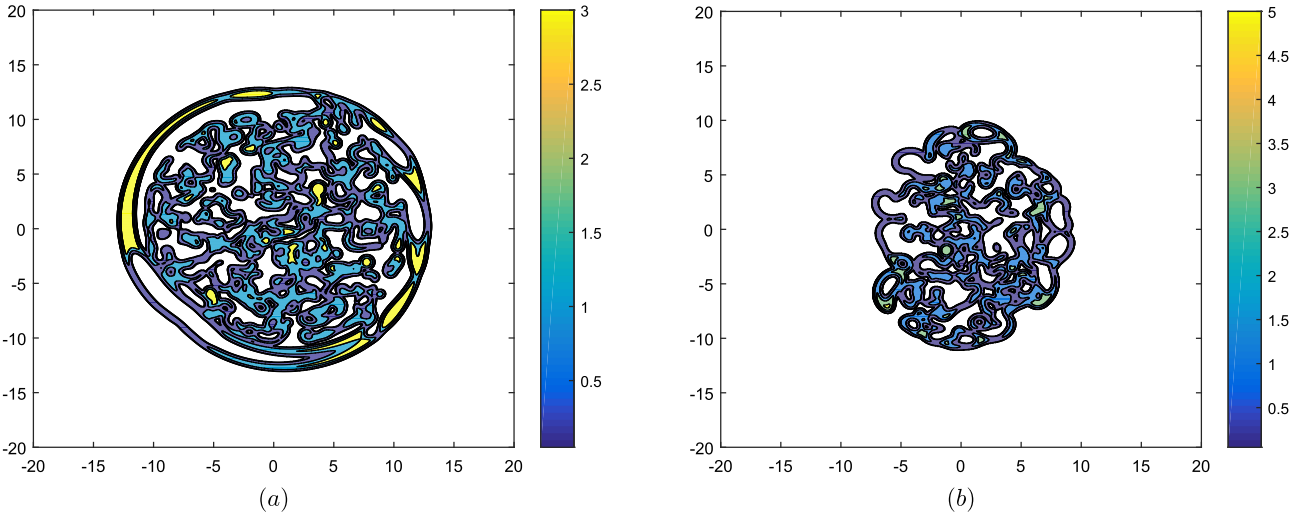

FIGURE 4. Asymmetric spatial patterns appearing from initial conditions (2.17)–(2.18) at time $t = 200$. (a) A convex population front obtained for $a = 4.0$ and $b = 0.76$. (b) A concave population front obtained for $a = 4.0$ and $b = 0.71$. In both cases, parameter values belong to Domain 3.

patches. The results shown in Figure 3 also demonstrate a complicated dependence of the spatial pattern on parameters a and b. For example, choosing $a = 5.1$ and decreasing b from $b = 0.704$ down to $b = 0.686$ will result in formation of a concave front for $b \in [0.7, 0.704]$ which will be replaced by patchy density distributions for $b \in [0.696, 0.7]$ followed by the extinction at $b \in [0.694, 0.696]$. We can then see formation of the concave front again for $b \in [0.690, 0.694]$ before the extinction occurs at $b \in [0.686, 0.690]$. To summarize, the concave continuous front topology prevails in Domain 3 of parametric plane (b, a) whilst the patchy invasion is relatively hard to generate as it only exist for $b \in [0.69, 0.73]$.

In the above simulations we used the symmetrical initial conditions (2.15)–(2.16). Now we are going to check the sensitivity of our results to the choice of the initial conditions. Obviously, the symmetry of the spatial patterns shown in Figure 2 is an artifact of the symmetric initial conditions; from the point of real ecological systems the symmetric patterns are somewhat artificial. The asymmetric initial conditions (2.17)–(2.18) result in more realistic asymmetric spatial patterns, see Figure 4 where the snapshots of the population density are shown at time $t = 200$. We immediately observe that the two baseline patterns of spread such as the convex front and concave front are present; however, they emerge for different parameter values. Hence our next goal is to check how the fine structure of Domain 3 may change if the initial conditions are chosen as given by (2.17)–(2.18).

Comparison between the results obtained for symmetric and asymmetric initial conditions is shown in Figure 5 where we use the same color coding as above; see Figure 3. As well as above, all the snapshots are analyzed at time $t = 200$. As generation of the maps in the parameter space is a computationally very expensive and time-consuming task, for the purpose of the comparison we select a small sub-domain $b \in [0.700, 0.712]$, $a \in [3.9, 4.9]$. The fine structure of the domain resulting from the symmetric initial conditions is shown in Figure 5a (which is a fragment of the larger map shown in Fig. 3), while the fine structure of the domain resulting from the asymmetric initial conditions is presented in Figure 5b. One immediate observation from Figure 5 is that there is little correspondence between Figures 5a and 5b (apart from the generic complexity of intermittent structure). We therefore conclude that, whether the population invades *via* the propagation of a concave continuous front or by the patchy spread (without a continuous front) depends not only on the value of the demographic parameters but also on the initial conditions. We also observe that breaking symmetry in the initial density distribution decreases the parameter range where the population goes to extinction. Also, the patchy spread occurs in a

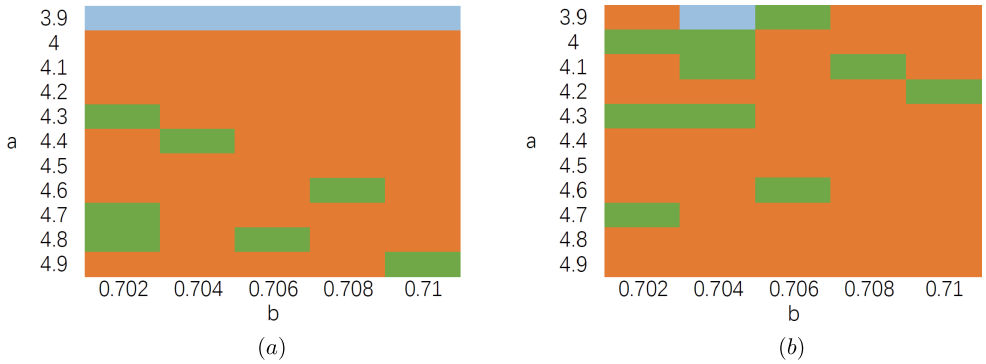

FIGURE 5. The structure of sub-domain $\mathcal{D}_1$ ($b \in [0.700, 0.712]$, $a \in [3.9, 4.9]$) of parameter plane (b, a) is shown for (a) symmetric initial conditions (2.15)–(2.16) and (b) asymmetric initial conditions (2.17)–(2.18). As well as in Figure 3, the topology of spatial density distributions is analyzed at time $t = 200$. See Figure 3 for the explanation of the colour coding.

somewhat wider range of parameters a and b when asymmetric initial conditions are implemented. Meanwhile a concave continuous front remains a dominant pattern of spread.

4. Results II: Sensitivity of spatial patterns to the cutoff

Now we are going to analyze the spatial patterns in more detail. As a starting point, we mention one particular feature of all snapshots of the population distribution shown in Figures 2 and 4. In the areas marked by white color, the population density is said to be zero. A question may arise here as to how that may be possible since the dispersal kernels (2.12) apparently make the population density positive everywhere in any generation starting from $t = 1$. A closer look into this apparent inconsistency immediately reveals that zero density is a result of visualization rather than a true property of the solution as any computer visualization program treats sufficiently small values as zeros. Hence a question may arise how much different the pattern shown by the "modified" solution with a cutoff at low densities can be from the pattern shown by the true solution.

The above issue is directly related to the accuracy of real-life ecological data. The matter is that very small values of the population density are often impossible to detect due to limitations of sampling/monitoring techniques, the minimum detectable density being called the "detection threshold". Hence, another reason to introduce the cut-off threshold density, say C, is to make our model consistent with a real-life monitoring routine.

Correspondingly, in this section we investigate the sensitivity of the spatial pattern to the cut-off parameter C. Moreover, since field data are often available not in the form of the population density distribution over space but as binary presence/absence maps (see the introduction for details), we consider the modified population distribution $\hat{N}$ as follows:

$$\hat{N}(x, y) = 1 \quad \text{for} \quad N > C, \qquad \hat{N}(x, y) = 0 \quad \text{for} \quad N \le C. \tag{4.1}$$

The specific question that we are going to consider is how the number of disconnected patches depends on the cutoff threshold C for different patterns of spread such as the concave front propagation and the patchy invasion.

In order to handle patchy spatial patterns, we use the Image Processing Toolbox (IPT) in MATLAB [24] to count number n of separate patches for a given value of C. Using the IPT software requires us to convert the original density distribution to a binary image as is described by equation (4.1). Two such binary images obtained at the cut-off value $C_0 = 0.05$ are shown in Figure 6 where we have a concave-front density pattern in Figure 6a and a patchy-invasion density pattern in Figure 6b. For the purpose of our study we ignore a complex

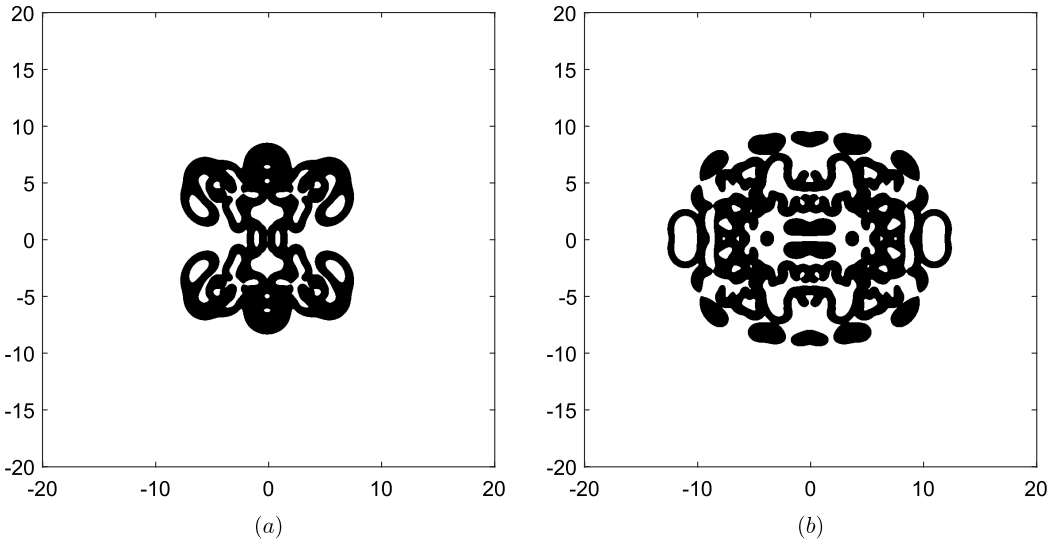

FIGURE 6. Binary "presence/absence" images, see equations (4.1), of spatial density distributions with a different topological structure. Both images are generated using the same cut-off threshold $C_0 = 0.05$. (a) A concave-front pattern obtained for parameters $a = 4.1$ and $b = 0.71$. (b) A patchy invasion pattern (with no continuous front) obtained for parameters $a = 4.0$ and $b = 0.73$. In both cases the parameters belong to Domain 3, the solution is shown at $t = 200$.

topological structure of the spatial density distribution within any sub-domain of the non-zero density with a closed boundary (*e.g.* density patterns behind a continuous front) as we are only interested in the number of separate patches. Thus, from a visual inspection we conclude that there is only one "object" (*i.e.* a region of the non-zero density with a closed external boundary) in the pattern shown in Figure 6a, but there are three separate objects in Figure 6b (note two small disconnected patches at the top and bottom of the pattern). This conclusion about the number of objects is confirmed by analyzing the images in the figure with help of the IPT MATLAB software.

Let us consider the concave-front pattern shown in Figure 6a. Because the pattern has a complicated structure, in particular contains many holes, it can be intuitively expected that a sufficiently large increase in the cut-off C should break the single object into a collection of multiple objects. Such a transformation indeed occurs and is shown in Figure 7a where the original concave density distribution is transformed to the binary image with $C = 0.840$. The spatial pattern that has originally been classified as a concave continuous front now turns into a patchy distribution consisting of five separate objects. Moreover, the number of objects will increase as the cut-off value is getting bigger. Transition from five to six objects as the cut-off is increased from $C = 0.840$ to $C = 0.865$ is shown in Figures 7a and 7b. Similarly, the number of separate patches is increased when we increase the cut-off for a patchy-invasion density distribution shown in Figure 6b. An increase in the cutoff value to $C = 0.08$ increases the number of disconnected objects to five (against three in the original pattern), see Figure 7c. A further increase to $C = 0.130$ increases this number to nine, see Figure 7d.

The above consideration apparently leads to a conclusion that the classification of spatial patterns made in the previous section (*e.g.* convex front *vs* "no-front" patchy invasion) does not make much sense because a concave-front spatial distribution can become a patchy-invasion-type distribution depending on the cut-off value. However, such a conclusion would be premature and, in fact, erroneous as the increase in the number of separate objects (patches) with an increase in the cutoff density C occurs in a significantly different manner for the concave-front and patchy invasion patterns, as is shown below.

Consider the concave-front pattern first. Let us gradually increase the cut-off density starting from the original value $C_0 = 0.05$ with an increment $\delta C = 0.001$ and count number n of separate objects when a concave density

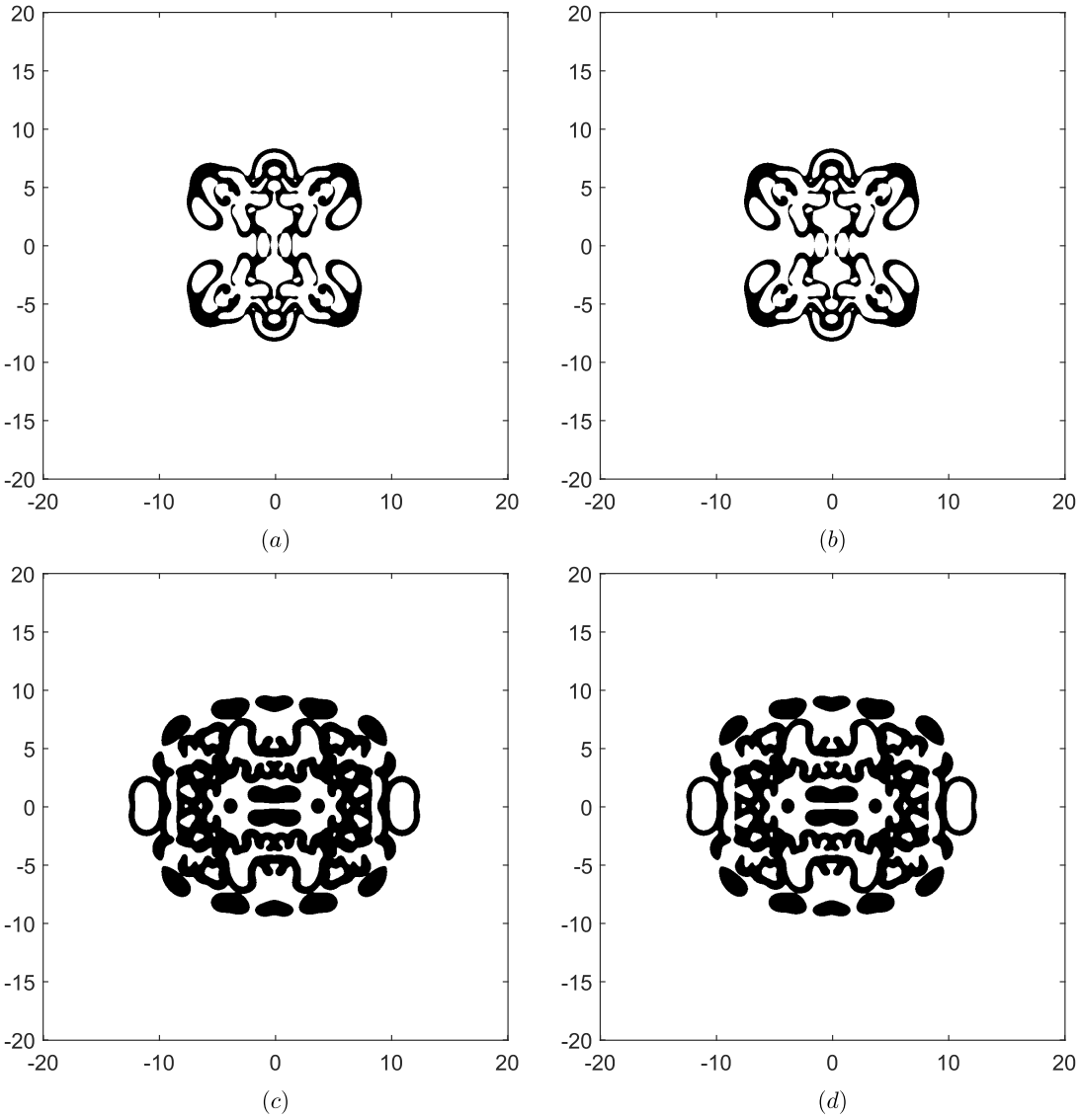

FIGURE 7. Decomposition of the spatial patterns shown in Figure 6 as a response to an increase in the cut-off threshold C. (a) $C = 0.840$; a concave continuous front pattern (see Fig. 6a) is transformed into a patchy distribution consisting of five disconnected patches. (b) $C = 0.865$; transition from five to six separate patches. (c) $C = 0.08$; a patchy-invasion density distribution (see Fig. 7b) has got five separate patches (compared to three in the original solution). (d) $C = 0.130$; transition from five to nine separate patches.

distribution in Figure 6a is considered. The results are presented in Table 1 where we notice that the concave distribution appears as a continuous front – *i.e.* one object, $n = 1$ – until the cut-off value is increased up to a rather high value $C = 0.826$ where a single object finally breaks into five disconnected patches.

Concave spatial patterns do appear as a single object for a wide range of cut-off values and we have observed this basic feature of concave density distributions in a number of numerical experiments. As an example, we show the results of our study for two other concave distributions obtained (at $t = 200$) for parameters $a = 6.0$,

TABLE 1. Transition from a continuous front distribution to a patchy distribution for the concave-front pattern when cut-off value C is varied with an increment of 0.001; n is the number of disconnected objects. Other parameters are $a = 4.1$, $b = 0.71$ and $t = 200$. Only those values of C are shown where the number of objects change.

C	0.05	$\cdots$	0.826	$\cdots$	0.858	$\cdots$	0.879	...	0.905	...	0.956
n	1	1	5	5	6	6	10	10	14	14	18

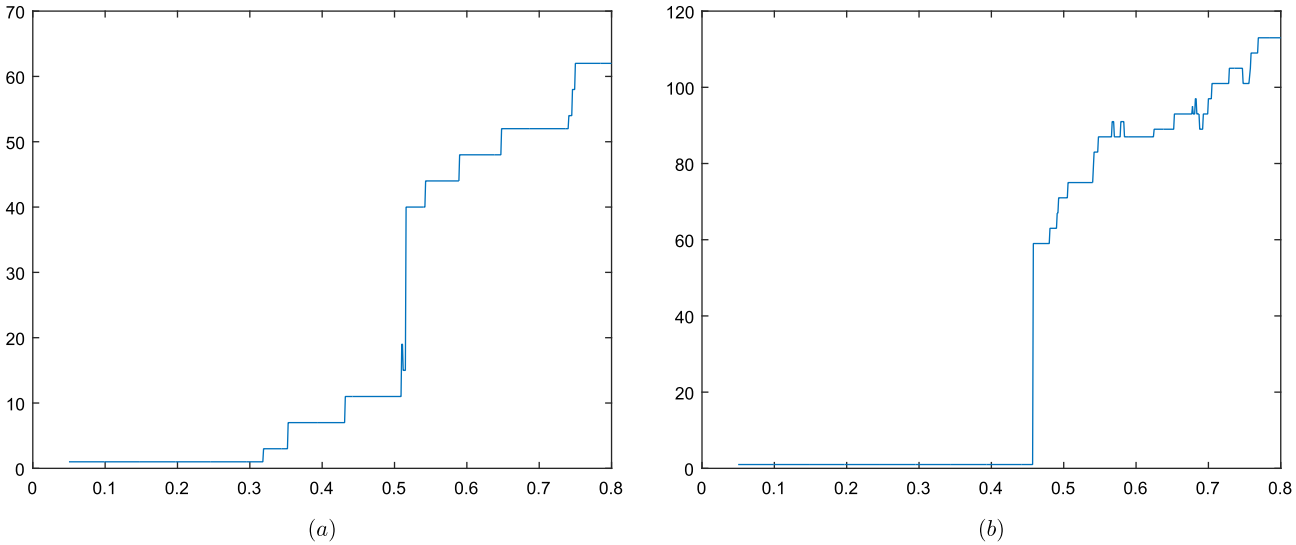

(a) (b)

FIGURE 8. The number of objects as a function of the cut-off value C for two concave-front distributions. Parameters are (a) $a = 6.0$, $b = 0.710$ and (b) $a = 5.7$, $b = 0.711$.

$b = 0.710$ and $a = 5.7$, $b = 0.711$. Graphs $n(C)$ are presented for those distributions in Figures 8a and 8b respectively. In both cases we have a broad range of cutoff values ($C \in [0.05, 0.32]$ in Fig. 8a and $C \in [0.05, 0.47]$ in Fig. 8b) where $n = 1$. Therefore, the concave continuous front is not broken until C becomes large. Meanwhile it is worth noticing that the details of the dependence $n(C)$ can be somewhat different: the number of patches increases gradually in Figure 8a, but there is a very sharp increase in the number of patches (from 1 to about 60) for the convex spatial pattern in Figure 8b. Another interesting observation is that function $n(C)$ is not necessary monotone as the number of objects can occasionally decrease for a higher cut-off value. This may happen when the maximum population density in small separate patches appears to be smaller than the value of the cutoff. One example is given by the peak in Figure 8a where a very slight increase in the cut-off value from $C = 0.511$ to $C = 0.512$ removes four objects from the spatial pattern and reduces the total number of objects from nineteen to fifteen. The further increase in the cut-off value results in a higher number of objects as can be seen in the figure.

We now analyze how the number of separate/disconnected objects depends on cut-off parameter C for the binary image shown in Figure 6b, *i.e.* in case of the patchy-invasion pattern. The results of the spatial pattern transformation when the cut-off value is increased are presented in Table 2. It is readily seen that the pattern transformation occurs in an essentially different way in comparison to a concave density distribution as already a small value of the cut-off results in a sharp increase in number n of separate patches. Whilst cut-off $C = 0.5$ (approximately 10% of the steady-state density) still retains a single object for the concave-front density distribution (see Tab. 1), the "no-front" patchy-invasion density distribution is already decomposed into fifteen separate objects (Tab. 2).

TABLE 2. Transitions of a patchy distribution in Figure 6b when the cut-off value C is varied; n is the number of disconnected objects. Only those values of C are shown where the number of objects change.

C	0.05	$\cdots$	0.065	$\cdots$	0.108	$\cdots$	0.157	$\cdots$	0.540	$\cdots$	0.584
n	3	3	5	5	9	9	13	13	15	15	19

Rapid changes in the topology of patchy spatial patterns are further confirmed by graphs $n(C)$ shown in Figure 9 that were obtained for three other patchy-invasion spatial patterns. It is readily seen that patchy distributions generated with various values of parameters a and b exhibit a similar response to an increase in the cut-off density. A relatively small number of patches observed at the original cut-off $C = 0.05$ is eventually transformed into a collection of a larger number of patches when C is getting larger. Importantly, the sharp increase in the number of patches consistently occurs for the values of the cutoff density several times smaller than it was observed for the concave-front patterns.

5. Discussion and concluding remarks

Understanding the properties of the spatiotemporal patterns of alien species spread during biological invasion is a problem of considerable theoretical and practical importance as it has implications for the invasive species management and control [18, 34]. The traditional view of the problem dating back to the seminal works by Fisher [6], Kolmogorov *et al.* [13] and Skellam [44] was based on the theoretical prediction of a circular front (in a 2D space) propagating away from the place of the species introduction [42, 46]. In a realistic non-uniform environment, the otherwise perfect circular shape may become distorted, *e.g.* see [2], but the existence of a continuous population front separating invaded area behind the front from non-invaded area in front of the front was thought to be a general property of the invasive spread. This view was eventually challenged by the discovery that the same growth-dispersal population models predict also an alternative scenario of "patchy invasion" where no continuous front exists and the alien species spread occurs through the formation and dynamics of patches of high population density [25, 26, 31, 32, 37].

Identification of the factors affecting the pattern of spread, *e.g.* continuous-front or patchy, and the knowledge of the structure of the corresponding parameter space is needed in the context of the invasive species monitoring as observing separate parches apparently requires a larger effort, more resources and, altogether, a significantly different monitoring strategy [34]. Meanwhile, such knowledge has been insufficient so far and mostly limited to the reaction-diffusion models [9, 30, 32]. In this paper, our goal was to address these issues in terms of the integral-difference modelling framework which is thought to be biologically more realistic than PDEs [14]. For this purpose, we considered a time-discrete space-continuous prey-predator/host-parasitoid system. Mathematically, the system is described by two coupled nonlinear integral-difference equations. We revealed three qualitatively different scenarios of spread, *i.e.*, by the propagation of a convex (continuous) front, propagation of a concave (continuous) front, and patchy spread. Having performed extensive computer simulations, we showed that the corresponding parameter space have a complicated "intermittent" structure, see Figures 3 and 5.

We mention here that species spread through the propagation of a continuous concave-shaped population front was earlier observed in a reaction-diffusion model of biological invasion [9] where it was branded as a "transitional" pattern between the convex front and the patchy spread. However, it remained unclear how this transition actually takes place. Here we addressed this issue (partially motivated by the widespread tendency to present empirical results as presence/absence data) by considering the sensitivity of the pattern's properties to the cutoff at low densities. We have shown that the spatial patterns resulting from the concave front propagation and from the patchy invasion respond differently to the value of the threshold density. In both cases, the number of disconnected patches increases along with an increase in the threshold density, such an increase starts when the threshold exceeds a certain critical value. However, the critical value of the threshold is consistently several times larger for the concave-front pattern than for the patchy-invasion pattern, even when visually the patterns

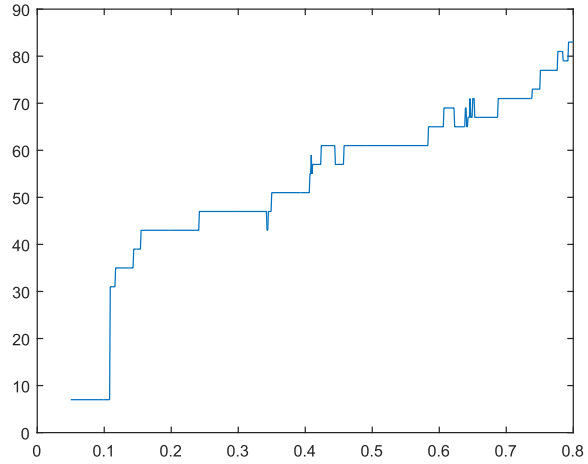

(a)

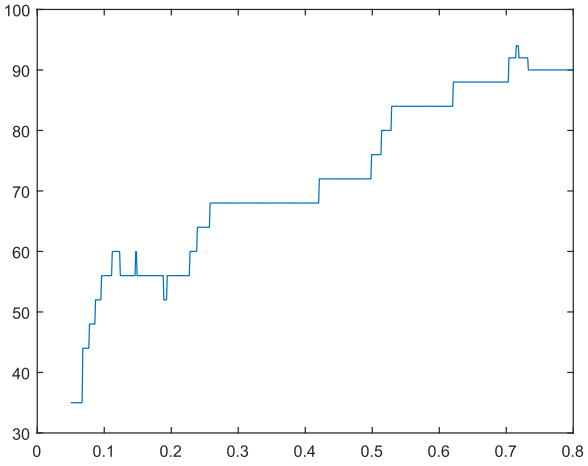

(b)

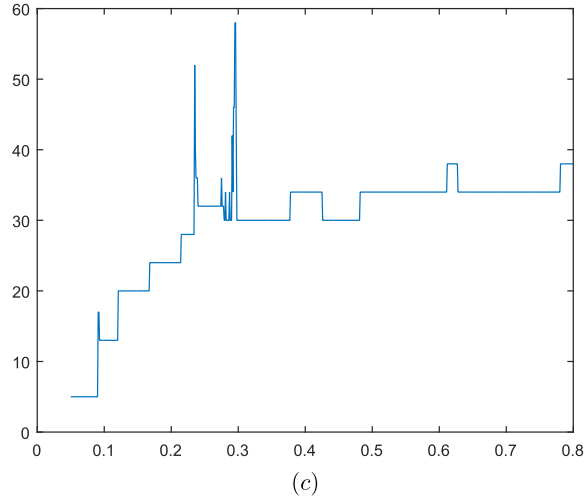

(c)

FIGURE 9. The number of objects as a function of the cut-off value for patchy distributions. Parameters are: (a) $a = 5.2$, $b = 0.71$, (b) $a = 6.4$, $b = 0.71$ and (c) $a = 5.9$ and $b = 0.71$.

may have similar properties. For this reason, the concave front propagation should be considered as a separate pattern rather than just a transition between the convex front propagation and the patchy invasion.

The much higher sensitivity of the patchy spread to the cutoff sends an important practical message to invasion managers about the type of field data needed for reliable monitoring and efficient control of invading species. Whilst the less expensive presence/absence data may provide an accurate representation of the spatial pattern emerging in case of the continuous front propagation, they are likely to give grossly distorted information in case of the patchy invasion. In the latter case, presence/absence data must be replaced by more expensive population density maps. Thus, a careful pre-assessment of the invasion scenario, which should include mathematical and statistical modelling, is required before deciding on an efficient monitoring protocol and control measures.

Acknowledgements. The first author (NBP) thanks Tilo Burghardt for drawing her attention to the MATLAB image processing package.

References

[1] L.J.S. Allen, An Introduction to Mathematical Biology. Pearson Prentice Hall, Upper Saddle River, NJ (2007).
[2] D.A. Andow, P.M. Kareiva, S.A. Levin and A. Okubo, Spread of invading organisms. *Landsc. Ecol.* **4** (1990) 177–188.
[3] M. Bengfort, H. Malchow and F.M. Hilker, The Fokker–Planck law of diffusion and pattern formation in heterogeneous environments. *J. Math. Biol.* **73** (2016) 683–704.
[4] M.B. Davis, R.R. Calcote, S. Sugita and H. Takahara, Patchy invasion and the origin of a Hemlock-Hardwoods forest mosaic. *Ecology* **79** (1998) 2641–2659.
[5] M. Fasham, The statistical and mathematical analysis of plankton patchiness. *Oceanogr. Mar. Biol. Ann. Rev.* **16** (1978) 43–79.
[6] R.A. Fisher, The wave of advance of advantageous genes. *Ann. Eugen.* **7** (1937) 355–369.
[7] D. Grünbaum, The logic of ecological patchiness. *Interface Focus* **2** (2012) 150–155.
[8] A. Hastings, S. Harisson and K. McCann, Unexpected spatial patterns in an insect outbreak match a predator diffusion model. *Proc. R. Soc. Lond. B* **264** (1997) 1837–1840.
[9] M. Jankovic and S.V. Petrovskii, Gypsy moth invasion in North America: a simulation study of the spatial pattern and the rate of spread. *Ecol. Compl.* **14** (2013) 132–144.
[10] M. Jankovic, S.V. Petrovskii and M. Banerjee, Delay driven spatiotemporal chaos in single species population dynamics models. *Theor. Popul. Biol.* **110** (2016) 51–62.
[11] D.M. Johnson, A.M. Liebhold, P.C. Tobin and O.N. Bjørnstad, Allee effects and pulsed invasion by the gypsy moth. *Nature* **444** (2006) 361–363.
[12] P.M. Kareiva, Population dynamics in spatially complex environments: theory and data. *Philos. Trans. R. Soc. Lond. B* **330** (1990) 175–190.
[13] A.N. Kolmogorov, I.G. Petrovskii and N.S. Piskunov, A study of the diffusion equation with increase in the quantity of matter, and its application to a biological problem. *Bull. Moscow Univ. Math. Ser. A* **1** (1937) 1–25.
[14] M. Kot and W.M. Schaffer, Discrete-time growth-dispersal models. *Math. Biosci.* **80** (1986) 109–136.
[15] S. Levin, Patchiness in marine and terrestrial systems: from individuals to populations. *Philos. Trans. R. Soc. B* **343** (1994) 99–103.
[16] S.A. Levin, T.M. Powell and J.H. Steele, Patch Dynamics, Lecture Notes in Biomath. Vol. 96. Springer-Verlag, Berlin (1993).
[17] M.A. Lewis and S. Pacala, Modeling and analysis of stochastic invasion processes. *J. Math. Biol.* **41** (2000) 387–429.
[18] M.A. Lewis, S.V. Petrovskii and J. Potts, The Mathematics Behind Biological Invasions. Interdisciplinary Applied Mathematics. Vol. 44. Springer, Berlin (2016).
[19] A.M. Liebhold, J.A. Halverson and G.A. Elmes, Gypsy moth invasion in North America: a quantitative analysis. *J. Biogeogr.* **19** (1992) 513–520.
[20] A.M. Liebhold *et al.*, Gypsy moth in the United States: An atlas. US Department of Agriculture. General Technical Report NE-233 (1996).
[21] F. Lutscher and S.V. Petrovskii, The importance of census times in discrete-time growth-dispersal models. *J. Biol. Dyn.* **2** (2008) 55–63.
[22] R.N. Mack, Invasion in *Bromus tectorum* L. into western North America: an ecological chronicle. *Agro-Ecosyst.* **7** (1981) 145–165.
[23] H. Malchow, S.V. Petrovskii and E. Venturino, Spatiotemporal Patterns in Ecology and Epidemiology: Theory, Models, Simulations. Chapman & Hall/CRC Press, Boca Raton (2008).
[24] https://uk.mathworks.com/help/images/index.html.
[25] D.C. Mistro, L.A.D. Rodrigues and S.V. Petrovskii, Spatiotemporal complexity of biological invasion in a space- and time-discrete predator–prey system with the strong Allee effect. *Ecol. Compl.* **9** (2012) 16–32.
[26] A.Y. Morozov, S.V. Petrovskii and B.L. Li, Spatiotemporal complexity of patchy invasion in a predator-prey system with the Allee effect. *J. Theor. Biol.* **238** (2006) 18–35.

[27] I.M. Parker, Mating patterns and rates of biological invasion. *PNAS* **101** (2004) 13695–13696.
[28] N. Petrovskaya and S.V. Petrovskii, Catching ghosts with a coarse net: use and abuse of spatial sampling data in detecting synchronization. *J. R. Soc. Interface* **14** (2017) 20160855.
[29] S.V. Petrovskii, Pattern, process, scale, and models sensitivity. *Phys. Life Rev.* **19** (2016) 131–134.
[30] S.V. Petrovskii and K. McKay, Biological invasion and biological control: a case study of the gypsy moth spread. *Asp. Appl. Biol.* **104** (2010) 37–48.
[31] S.V. Petrovskii, A.Y. Morozov and E. Venturino, Allee effect makes possible patchy invasion in a prey-predator system. *Ecol. Lett.* **5** (2002) 345–352.
[32] S.V. Petrovskii, H. Malchow, F.M. Hilker and E. Venturino, Patterns of patchy spread in deterministic and stochastic models of biological invasion and biological control. *Biol. Invas.* **7** (2005) 771–793.
[33] S.V. Petrovskii, D. Bearup, D.A. Ahmed and R. Blackshaw, Estimating insect population density from trap counts. *Ecol. Compl.* **10** (2012) 69–82.
[34] S.V. Petrovskii, N.B. Petrovskaya and D. Bearup, Multiscale approach to pest insect monitoring: random walks, pattern formation, synchronization, and networks. *Phys. Life Rev.* **11** (2014) 467–525.
[35] T. Powell, Physical and biological scales of variability in lakes, estuaries and the coastal ocean, edited by T. Powell and J. Steele. *Ecological Time Series*. Chapman & Hall, New York (1995), 119–138.
[36] L.A.D. Rodrigues, D.C. Mistro and S.V. Petrovskii, Pattern formation in a space- and time-discrete predator–prey system with a strong Allee effect. *Theor. Ecol.* **5** (2012) 341–362.
[37] L.A.D. Rodrigues, D.C. Mistro, E.R. Cara, N.B. Petrovskaya and S.V. Petrovskii, Patchy invasion of stage-structured alien species with short-distance and long-distance dispersal. *Bull. Math. Biol.* **77** (2015) 1583–1619.
[38] L.A. Segel and J.L. Jackson, Dissipative structure: an explanation and an ecological example. *J. Theor. Biol.* **37** (1972) 545–559.
[39] A.A. Sharov, A.M. Liebhold and E.A. Roberts, Correlation of counts of gypsy moths (Lepidoptera: Lymantriidae) in pheromone traps with landscape characteristics. *For. Sci.* **43** (1997) 483–490.
[40] J.A. Sherratt, M.A. Lewis and A.C. Fowler, Ecological chaos in the wake of invasion. *Proc. Natl. Acad. Sci. USA* **92** (1995) 2524–2528.
[41] J.A. Sherratt, B.T. Eagan and M.A. Lewis, Oscillations and chaos behind predator-prey invasion: mathematical artifact or ecological reality? *Philos. Trans. R. Soc. Lond. B* **352** (1997) 21–38.
[42] N. Shigesada and K. Kawasaki, Biological Invasions: Theory and Practice. Oxford University Press, Oxford (1997).
[43] N. Shigesada, K. Kawasaki and Y. Takeda, Modeling stratified diffusion in biological invasions. *Am. Nat.* **146** (1995) 229–251.
[44] J.G. Skellam, Random dispersal in theoretical populations. *Biometrika* **38** (1951) 196–218.
[45] C.F.G. Thomas, L. Parkinson and E.J.P. Marshall, Isolating the components of activity-density for the carabid beetle Pterostichusme lanarius in farmland. *Oecologia* **116** (1998) 103–112.
[46] V. Volpert and S.V. Petrovskii, Reaction-diffusion waves in biology. *Phys. Life Rev.* **6** (2009) 267–310.
[47] X. Wang, F.G. Blanchet and N. Koper, Measuring habitat fragmentation: an evaluation of landscape pattern metrics. *Meth. Ecol. Evol.* **5** (2014) 634–646.